Drivers of water storage changes in the Yangtze River Basin during 2002-2022

Jielong Wang[1], Yunzhong Shen[1,*], Joseph Awange[2], Natthachet Tangdamrongsub[3], Tengfei Feng[1], Ling Yang[1], Yongze Song[4]

[1] College of Surveying and Geo-informatics, Tongji University, Shanghai, 200092, PR China

[2] School of Earth and Planetary Sciences, Spatial Sciences Discipline, Curtin University, Perth, WA, Australia

[3]Water Engineering and Management, School of Engineering and Technology, Asian Institute of Technology, Pathum Thani 12120, Thailand

[4] School of Design and the Built Environment, Curtin University, GPO Box U1987, Perth, WA 6845, Australia

* Corresponding author: Yunzhong Shen (yzshen@tongji.edu.cn)

Key Points:

- The apparent upward trend in total water storage (TWS) within the Yangtze River Basin (YRB) cannot be directly attributed to precipitation.
- Groundwater accumulation is a primary factor contributing to the increase in TWS across much of YRB.
- The increase in surface water storage in YRB is primarily driven by the rising number of reservoirs.

Abstract

The Yangtze River Basin (YRB), home to around 400 million people, boasts of abundant water resources and significant spatial heterogeneity. Revealing the driving factors of water storage changes in YRB is essential for effective water resource management and sustainable development. In this study, we assess the drivers of total water storage (TWS) changes derived from the Gravity Recovery and Climate Experiment (GRACE) satellite within YRB from two perspectives: water balance and water storage components, including snow water equivalent (SWE), surface water storage (SWS), soil moisture storage (SMS), and groundwater storage (GWS). We also investigate the influence of reservoirs (e.g., Three Gorges Reservoir (TGR)), lakes (e.g., Dongting, Poyang, and Taihu), and glacier thawing on regional TWS changes. The results reveal an apparent increasing trend in YRB's TWS from 2002 to 2022, while trends in precipitation, evapotranspiration, and runoff do not adequately account for this observed trend. In addition, our findings show that the increased TWS primarily occurs during the non-monsoon season, characterized by limited precipitation. The analysis of water components shows that the rise in TWS within YRB is predominantly attributed to GWS accumulation. SWS also contributes to the increasing TWS, primarily driven by the reservoir filling. The filling of TGR explains the observed TWS increase in Hubei province, whereas Lake Poyang accounts for about 30% of the positive TWS trend in Jiangxi province. Our comprehensive analysis systematically unveils the drivers of water storage changes in YRB, providing valuable insights for its sustainable water resource management and utilization.

Keywords: GRACE; water balance equation; water storage components; groundwater accumulation

1. Introduction

Recognized as one of China's most significant cultural and socioeconomic regions, the Yangtze River Basin (YRB) plays a critical role in national water resource management and ecological conservation (Chao et al., 2023). This region is densely populated and of great importance, with an annual average water resource of about 995.5 billion cubic meters, of which over 200 billion cubic meters are allocated for water supply (Wang et al., 2023). Nevertheless, the Yangtze River remains one of the world's top ten rivers in terms of water scarcity (Dai et al., 2008). This is primarily due to the escalating water requirements for agricultural purposes, industrial activities, energy generation, and drinking water within this basin (Yang et al., 2015). Over the past few decades, human activities and climate change have joint forces to significantly alter the hydrological cycle of YRB, resulting in a higher frequency of floods and droughts in this region (Shan et al., 2018; Yang et al., 2021b; Wang and Chen, 2022; Xie et al., 2022). For example, the abnormal heat waves during the summer of 2022 led to long-lasting droughts that severely affected YRB (Lu et al., 2022). Conversely, the summer of 2020 witnessed historic floods in the basin, which had catastrophic socioeconomic consequences (Zhou et al., 2021; Yan et al., 2022). As a result, over the past half-century, more than 50 thousand reservoirs have been built to regulate river flows and secure adequate water supply in YRB. These reservoirs collectively impounded nearly 360 billion cubic meters of water in 2021 (Ministry of Water Resources of the People's Republic of China). In addition, many valuable freshwater resources (e.g., lakes) are readily accessible for human consumption. Therefore, understanding the drivers of water storage changes in YRB can inform sustainable water management practices, help mitigate the impact of water scarcity, and ensure the basin's long-term environmental and economic stability.

Since its launch in 2002, the Gravity Recovery and Climate Experiment (GRACE) satellites have provided invaluable observations, i.e., total water storage (TWS), for investigating global or regional water availability and distribution (Tapley et al., 2019; Gao et al., 2021). Changes in TWS reflect the changes in regional mass redistribution and hydrological cycles from both natural variability and anthropogenic activities (e.g., Awange et al., 2013; Felfelani et al., 2017; Hosseini-Moghari et al., 2020), which can be used to characterize droughts and floods (see e.g., Long et al., 2014; Thomas et al., 2014; Tangdamrongsub et al., 2016; Xie et al., 2022; Zheng et al., 2023), monitor groundwater depletion (e.g., Agutu et al., 2019; Frappart et al., 2019; Feng et al., 2022), and close the terrestrial water budget (Chen et al., 2020; Rodell & Reager, 2023).

To date, GRACE-derived TWS observations have been applied to numerous river basins worldwide (e.g., Awang et al., 2011; Tangdamrongsub et al., 2015; Zhang et al., 2023), among which YRB was one of the most extensively examined regions regarding spatiotemporal dynamics of TWS (e.g., Huang et al., 2015; Sun et al., 2018; Wang et al., 2020; Xie et al., 2022). Nevertheless, previous studies predominantly concentrated on delineating and characterizing droughts and floods within this region. Due to the confluence of anthropogenic activities and the impacts of climate change, YRB has experienced a significant upward trend in TWS over recent years (Chao et al., 2023; Xu et al., 2023). However, the drivers behind this trend have remained a subject of limited exploration in prior research endeavors. Huang et al. (2015) indicated that the observed trends in TWS over YRB were highly likely due to the anthropogenic interventions in the hydrological cycle rather than natural climate variability. However, their investigation only presented the qualitative results for three specific regions within YRB, leaving systematic and quantitative analysis of the whole basin absent.

GRACE-derived TWS encompasses all terrestrial water components such as snow, ice, surface water (e.g., lakes and reservoirs), soil moisture, and groundwater. Global hydrological or land surface models have been commonly used (Feng et al., 2022; Schumacher et al., 2018) to discern these distinct water components. The results of Chao et al. (2021) showed that respective contributions of glaciers, surface water, soil moisture, and groundwater to TWS changes over YRB for the period 2002-2015 amounted to 15%, 12%, 25%, and 48%, respectively. In their subsequent investigation (Chao et al., 2023), they further elucidated that precipitation, evapotranspiration, and runoff collectively account for approximately 46%, 27%, and 27% of the variations in TWS within YRB, respectively. However, the factors driving the changes in the trend of YRB's TWS and its components were not discussed. Furthermore, TWS over YRB exhibits a heterogeneous spatiotemporal variability owing to its complicated topography and landscapes. The source region of YRB starts from the Tibetan Plateau, where glacier retreat, snowmelt, permafrost degradation, and lake expansion have had a significant impact on TWS due to global warming (Chao et al., 2020; Deng et al., 2022; Li et al., 2023). In the middle-lower reaches of the basin, numerous lakes and reservoirs, including the three largest freshwater lakes (Poyang, Taihu, and Dongting), Three Gorges Reservoir (TGR), and the Danjiangkou Reservoir (i.e., the origin for the Middle-Line South-to-North Water Diversion Project), are present. Although previous studies have independently reported their contributions to TWS changes within YRB (Wang et al., 2011; Long et al., 2020; Xu et al., 2020; Chao et al., 2023), a comprehensive, integrated and updated analysis is still lacking.

A wealth of multisource data, including satellites, reanalysis data, hydrological models, and in-situ observations, enables a more comprehensive and holistic view of hydrological processes (e.g., Awang et al., 2014; Awange et al., 2019; Arsenault et al., 2020; Awange, 2020; Awange, 2021; Chao et al., 2023; Feng et al., 2023; Li et al., 2023). Meanwhile, integrating these diverse datasets instills robust confidence, providing a solid foundation for facilitating evidence-based decision-making in environmental policies. However, previous studies lacked a mutual verification process with multiple datasets before assessing changes in TWS within YRB. Therefore, the reliability of the research findings needs further validation. In this study, each data employed will undergo a validation procedure to enhance the robustness and reliability of our findings, contributing to the overall credibility of the study. Subsequently, we aim to reveal the drivers of YRB's TWS from two perspectives: water balance and water storage components. This multifaceted approach enables a comprehensive understanding of the intricate processes influencing YRB's TWS, providing valuable insights for future advancements in water resource management.

2. Study area

The Yangtze River, also known as the Changjiang River, is the longest river in China and the third longest in the world. It stretches over 6300 kilometers from its source in the Tibetan Plateau to its mouth at the East China Sea (Fig. 1). YRB covers an area of approximately 1.8 million square kilometers and 19 provincial administrative regions (Table 1), accounting for approximately 20% of China's territory. Additionally, YRB contributes about 40% of China's total GDP (Li et al., 2021). Due to the influence of the East Asian Summer Monsoon and the South China Sea Summer Monsoon, annual precipitation in YRB is lower in the north than in the south, decreasing from southeast to northwest. In contrast, the annual temperature is higher in the east than in the west, increasing from north to south (Sun et al., 2018).

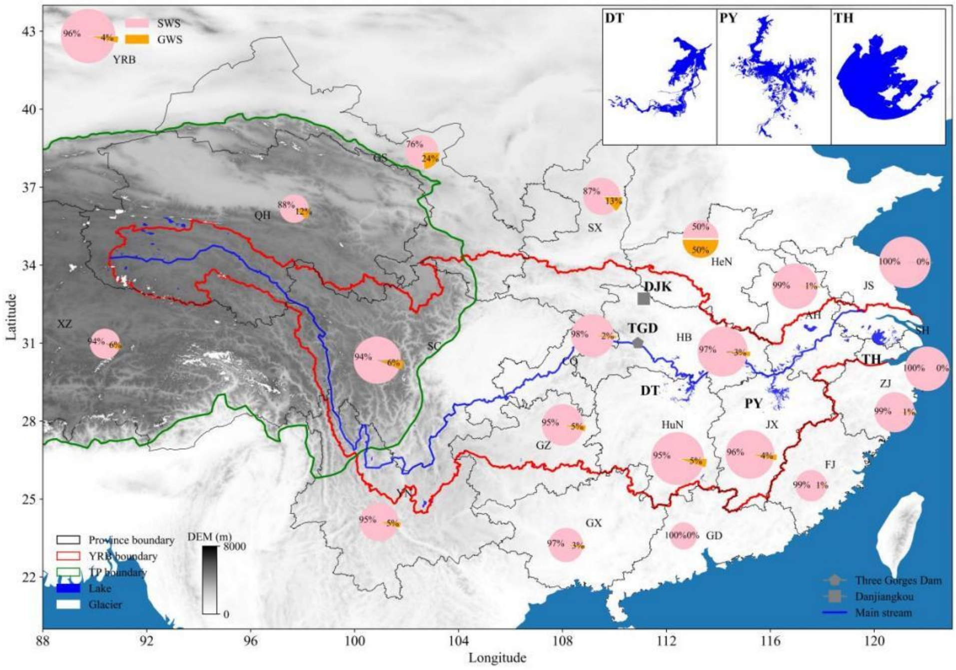

Fig. 1. Map of the Yangtze River Basin (YRB) in China, with streams, lakes, the Three Gorges Dam (TGD), and Danjiangkou (DJK) reservoir. The green line represents the boundary of the Tibetan Plateau (TP), with glaciers denoted in white. To the upper right of the figure, an enlarged view is provided of the three largest lakes: Dongting (DT), Poyang (PY), and Taihu (TH). The pie chart depicts the proportion of surface water and groundwater sources supplied from provincial-level administrative regions within YRB. The larger size of the chart indicates a greater volume of total water supply to YRB. These proportions are derived from the data provided by Ministry of Water Resources of the People's Republic of China from 2003 to 2021.

Surface water bodies, notably lakes and reservoirs, provide valuable water resources within YRB. In general, most lakes are situated in the regions of Qinghai, Hunan, Hubei, Jiangxi, and certain coastal cities (Fig. 2a), whereas reservoirs are distributed in the middle and lower reaches of YRB (Fig. 2b). Due to the rapid expansion of population and economic development, the aggregate water demand (i.e., domestic, agricultural, industrial, and environmental water use) in YRB has exhibited a substantial increase, surging from approximately 170 billion cubic meters in 2003 to 214 billion cubic meters in 2022 (Ministry of Water Resources of the People's Republic of China). It is noteworthy that nearly 96% of the region's water supply is sourced from surface water resources, while groundwater contributes relatively high in the provinces of Gansu, Shanxi, and Henan (Fig. 1). Grain production in YRB accounts for approximately 40% of the total production in China, which commands more than half of the total water consumption within the region (Long et al., 2015). Predominantly, irrigation practices are concentrated in the middle and lower regions of YRB, where a substantial portion of the land is irrigated utilizing surface water sources (Figs. 2c-d).

While much research has been conducted on TWS in YRB at various watershed scales, few studies have performed the analysis at the provincial level. Therefore, in this study, we divide YRB into nine sub-regions (Table 1) by merging specific adjacent provinces or autonomous regions while also considering the footprint of GRACE. We have omitted the provinces of Guangdong and Fujian from further analysis due to their relatively minor spatial extent within YRB.

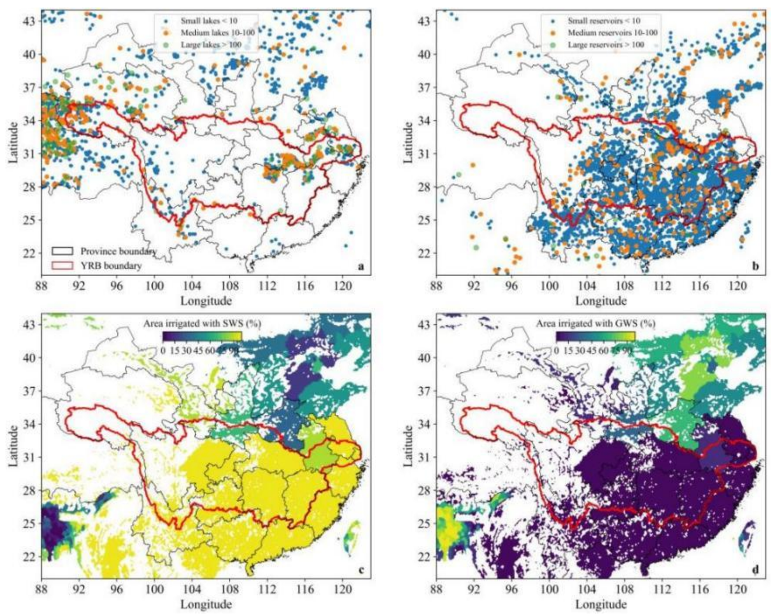

Fig. 2. (**a**) Distribution of large, medium, and small lakes derived from the China Lake Dataset for the year 2020 (Zhang et al., 2019a), and (**b**) large, medium, and small reservoirs derived from GeoDAR (Wang et al., 2022). Area irrigated with (**c**) surface water and (**d**) groundwater expressed as a percentage of total area equipped for irrigation from WGHM.

Table 1. Information of the 19 provincial administrative regions and specific study regions within YRB.

Administrative Regions (Abbr.)	Area, 10^4 km^2	Area within YRB, 10^4 km^2	Proportion of YRB, %	Study regions (Abbr.)
Chong Qing (CQ)	8.24	8.24	4.58	Chong Qing (CQ)
Guang Xi (GX)	23.76	0.86	0.48	GX-HuN (GH)
Hu Nan (HuN)	21.18	20.68	11.49	
Gan Su (GS)	42.58	3.63	2.02	GS-HeN-SX (GHS)
He Nan (HeN)	16.7	2.75	1.53	
Shan Xi (SX)	20.56	7.09	3.94	
Gui Zhou (GZ)	17.62	11.57	6.43	Gui Zhou (GZ)
Hu Bei (HB)	18.59	18.44	10.25	Hu Bei (HB)
Jiang Xi (JX)	16.69	16.31	9.06	Jiang Xi (JX)
Jiang Su (JS)	10.72	3.89	2.16	JS-ZJ-SH-AH (JZHW)
Zhe Jiang (ZJ)	10.55	1.41	0.78	
Shang Hai (SH)	0.63	0.63	0.35	
An Hui (AH)	14.01	6.60	3.67	
Qing Hai (QH)	72.23	15.84	8.80	Qing Hai (QH)
Si Chuang (SC)	48.6	46.70	25.94	SC-XJ-YN (SXY)
Xi Zang (XZ)	122.84	4.30	2.39	
Yun Nan (YN)	39.41	10.90	6.06	
Fu Jiang (FJ)	12.4	0.12	0.06	Discarded
Guang Dong (GD)	17.98	0.05	0.03	Discarded

3. Materials and Method

3.1. Data and processing

Table 2 summarizes the datasets used in this study and their respective origins, including GRACE/GRACE-FO data, hydrological data, water storage components, and other supplementary data. When necessary, the data is resampled to 0.25-degree grid space to ensure a consistent spatial resolution required for analysis.

3.1.1. GRACE and GRACE-FO data

GRACE/GRACE-FO was a joint satellite mission between the National Aeronautics and Space Administration (NASA) and the German Aerospace Centre (DLR), with the primary objective of monitoring the time variable gravity field. This field reflects the monthly redistribution of Earth's mass, which is dominated by hydrology (Tapley et al., 2019). GRACE provides gravity data from April 2002 to October 2017 (during its lifetime), while GRACE-FO continues to provide data since May 2018. In this study, mascons data from the Center for Space Research (CSR), Jet Propulsion Laboratory (JPL), and Goddard Space Flight Center (GSFC) are employed. It's worth noting that the gain factors provided with JPL mascons are used to restore much of the lost signal within YRB (Scanlon et al., 2016). The examination in Fig. S1 reveals notable correlations and minimal discrepancies among these three products in YRB. As a result, their ensemble is employed for our analysis.

3.1.2. Hydrological data

In a given river basin, the total water storage changes (TWSC) can be determined by the rate balance between precipitation (P), evapotranspiration (ET), and runoff (R) via the water balance equation as (Chen et al., 2020). We have compared the precipitation series from the Climate Research Unit (CRU) gridded Time-Series datasets (Harris et al., 2020), the NOAH model from the Global Land Data Assimilation System (GLDAS, Beaudoing & Rodell, 2020), and NOAA Climate Prediction Center (CPC, Xie et al., 2007). The results reveal high correlations observed among the three types of precipitation data (Fig. S2), and thus, their ensemble is used in this study. Nevertheless, less agreement was found in evapotranspiration and runoff datasets (Chen et al., 2020; Long et al., 2014). We have compared the evapotranspiration series from NOAH, the European Centre for Medium-Range Weather Forecasts (ECMWF) Re-Analysis (ERA5, Muñoz-Sabater, 2019), and the Global Land Evaporation Amsterdam Model (GLEAM, Martens et al., 2017), as well as the runoff series from NOAH, ERA5, and the Catchment Land Surface Model (CLSM) from GLDAS. While high correlations are observed among these datasets, they show relatively large differences regarding the amplitude (Fig. S3 and Fig. S4).

To identify the most suitable evapotranspiration and runoff products for use in this study, we conduct a comparative analysis of TWSC derived from GRACE against water balance estimates, which involves systematically testing various combinations of these products. As illustrated in Fig. S5 and Fig. S6, TWSC derived from the water balance equation using the CLSM's runoff data consistently exhibits high consistency with that derived from GRACE, regardless of the specific evapotranspiration products employed. Hence, we employ the runoff data from CLSM and the ensemble evapotranspiration from the three sources in this study.

3.1.3. Water storage components

As the contribution of the vegetation water storage is negligible over YRB (Wang et al., 2020), GRACE-derived TWS can be taken to be the summation of snow water equivalent (SWE), surface water storage (SWS), soil moisture storage (SMS), and groundwater storage (GWS) (Wang et al., 2020) as:

$$\mathrm{TWS} = \mathrm{SWE} + \mathrm{SWS} + \mathrm{SMS} + \mathrm{GWS} \tag{1}$$

Compared with the dataset of long-term series of snow depth in China, initially developed by Che et al. (2015) using passive microwave remote-sensing data, SWE sourced from NOAH exhibits reliable performance within YRB (Fig. S7). Meanwhile, SMS obtained from NOAH correlates well with that obtained from ERA5 (Fig. S8). Therefore, NOAH-derived SWE and the ensemble SMS derived from NOAH and ERA5 are used for further analysis.

Nevertheless, SWS and GWS persist as two of the most underrepresented or unrepresented components in hydrological models (Beaudoing & Rodell, 2020). The WaterGAP Global Hydrology Model (WGHM), subject to continuous refinement since 1996, has been employed to quantify human use of groundwater and surface water (Müller et al., 2021). The observed agreement between GRACE-derived TWS and WGHM-derived TWS demonstrates the model's efficacy over YRB (Fig. S9). In addition, reservoir water storage derived from WGHM shows a pronounced upward trend, aligning with the notable increase in reservoirs within YRB (Fig. S10b). SWS derived from WGHM shows consistent spatial distribution with the map of lakes and reservoirs (Fig.2 and Figs. S10a-c) and correlates well with the surface water resources data provided by the Ministry of Water Resources of the People's Republic of China (Fig. S11). Therefore, we utilize the SWS data sourced from WGHM, while GWS is determined using equation (5) by deducting other components from TWS.

3.1.4. Ancillary data

Annual water use data in terms of various water sources (i.e., SWS and GWS) and sectors (agricultural, domestic, industrial, and environmental use) are derived from the Bulletin of Water Resources in the Yangtze River Basin and Southwest Rivers (Ministry of Water Resources of the People's Republic of China). Lakes and reservoirs data are obtained from the China Lake Dataset (Zhang et al., 2019a) and GeoDAR (Wang et al., 2022), respectively. The in-situ daily water level data of the TGR and Danjiangkou Reservoir are sourced from the Hubei Water Resources Commission (https://slt.hubei.gov.cn/sjfb). Water level collected at Chenglingji and Hukou stations that are used to calculate the volume anomalies of Lake Dongting and Lake Poyang, respectively, is provided by the Hydrology Bureau of the Changjiang Water Resources Commission, China (http://www.cjh.com.cn). Lake Taihu's water level is downloaded from the Taihu Laboratory for Lake Ecosystem Research (http://thl.cern.ac.cn). Furthermore, the altimetry satellite-derived water level from the Database for Hydrological Time Series of Inland Waters (DAHITI, https://dahiti.dgfi.tum.de/en) and Hydroweb (https://hydroweb.theia-land.fr/) are employed for comparison analysis. The glacier runoff data from 2003 to 2015 is sourced from Wang et al. (2021).

Table 2. Datasets used in this study

Dataset	Variable	Time span	Resolution, °	Data source	Reference
JPL RL06.1Mv03			0.5	https://podaac.jpl.nasa.gov/dataset/TELLUS_GRAC-GRFO_MASCON_GRID_RL06.1_V3	Wiese et al. (2019)
CSR RL06.2M	TWS		0.25	https://www2.csr.utexas.edu/grace/RL06_mascons	Save et al. (2016)
GSFC RL06v2.0			0.5	https://earth.gsfc.nasa.gov/geo/data/grace-mascons	Loomis et al. (2019)
CRU V4.07	P, T		0.5	https://crudata.uea.ac.uk/cru/data/hrg/cru_ts_4.07	Harris et al. (2020)
CPC Global Precip	P	2002-2022	0.5	https://www.psl.noaa.gov/data/gridded/data.cpc.globalprecip	Xie et al. (2007)
ERA5-Land	ET, R, SMS		0.1	https://doi.org/10.24381/cds.68d2bb30	Muñoz-Sabater. (2019)
NOAH V2.1	P, ET, R, SWE, SMS		0.25	https://ldas.gsfc.nasa.gov/gldas	Rodell et al. (2004)
CLSM V2.1	R, SWE, SMS		1		
WGHM V2.2d	SWS	2002-2019	0.5	https://doi.pangaea.de/10.1594/PANGAEA.918447	Müller et al., 2021
GLEAM v3.8a	ET	2002-2022	0.25	https://www.gleam.eu/#downloads	Martens et al. (2017)
China snow depth	SD	2002-2021	0.25	https://doi.org/10.11888/Geogra.tpdc.270194	Che et al. (2015)
Glacier runoff dataset	Glacier	2003-2015	-	https://data.tpdc.ac.cn/zh-hans/data/b33dc082-b899-4ee1-8942-d0b5962e4e7f	Wang et al. (2021)
China Lake Dataset	Lake	2020	-	https://data.tpdc.ac.cn/en/data/fa8426c0-d3f0-4615-8e78-0465a0957891/	Zhang et al., 2019a
GeoDAR	Res	-	-	https://zenodo.org/records/6163413	Wang et al. (2022)
TGR, DJK				https://slt.hubei.gov.cn/sjfb	-
CLJ, HK	Water level	2003-2021	-	http://www.cjh.com.cn	
DAHITI				https://dahiti.dgfi.tum.de/en	-
Hydroweb				https://hydroweb.theia-land.fr/	-

3.2. Method

3.2.1. Analyzing trends in hydrological data, TWS and its components

The spatiotemporal trends of hydrological data and water storage are detected by the nonparametric Mann-Kendall test, which does not require distributional assumptions about the time series and is robust against outliers and missing values (Panda & Wahr, 2016; Zhu et al., 2021). It has been recommended by the Intergovernmental Panel on Climate Change (IPCC) to be applied in a series of environmental, climate, and hydrological data (Meshram et al., 2020). The

Mann-Kendall test statistic S is calculated as (Liu et al., 2021):

$$S = \sum_{i=1}^{n-1} \sum_{j=i+1}^{n} \operatorname{sgn}(x_i - x_j) \quad (4)$$

where x is the examined time series, n is the number of observations, and sgn is the indicator function. For large sample sizes ($n > 10$), the test statistic Z_{MK} is distributed approximately normally:

$$Z_{MK} = \begin{cases} \frac{S-1}{\sqrt{Var}}, & if\ S > 0 \\ 0, & if\ S = 0 \\ \frac{S+1}{\sqrt{Var}}, & if\ S < 0 \end{cases} \quad (5)$$

where $\sqrt{\mathrm{Var}}$ is the variance of S. If Z_{MK} is greater than 0, the data shows an increasing trend, while the data shows a decreasing trend if Z_{MK} is less than 0. The significance test is calculated using the Man-Kendall test with p-value < 0.05, whereas the magnitude of the trend is estimated using the Theil-Sen's method (Seka et al., 2022). Prior to computing trends, the seasonal cycle is removed following Rodell et al. (2018)'s method.

3.2.2. Assessing the role of water components in TWS

To quantify the contribution of individual water components to TWS, components contribution ratios (CCR) are used in this study as follows (Wang et al., 2020):

$$CCR_s = \frac{MAD_s}{TV} \quad (6)$$

where $MAD_s = \frac{1}{N}\sum_t^n \left|S_t - \overline{S}\right|$ is the mean absolute deviation (MAD) of a single storage component, while $TV = \sum_s^{storages} MAD_s$ is total variability (TV), which is the summation of MAD of each component. The subscript s denotes individual water components (i.e., SWS, SWE, SMS, and GWS) and N is the number of samples. The higher the CCR, the more significant the component's role in TWS.

3.2.3. Estimating volume anomalies in large reservoirs and lakes

The volume of the specified reservoirs and lakes is derived using the water level-volume relationship. In particular, the volume V (km^3) of TGR is derived using the in-situ water level H (m) data ($V = 0.2968 \times 1.0284^{H}$, $R^2 = 0.999$) (Wang et al., 2011). The volume of Lake Dongting and Lake Poyang is estimated using the water level at Chenglingji station (Yang et al., 2021a, $R^2 = 0.82$) and Hukou station (Liu et al., 2013; Liu et al., 2020, $R^2 = 0.86$), respectively. The volume of Taihu Lake is obtained using the water level data, following Zhang et al. (2013) ($R^2 = 0.99$). Volume anomalies are derived by removing the 2004-2009 mean field.

4. Results

4.1. Trends in TWS and water balance components

Figure 3a illustrates a generally coherent increase in TWS within YRB in contrast to apparent negative trends observed over the North China Plain and Eastern Indian Region. These upward trends are particularly pronounced in Sichuan, Chongqing, and Guizhou provinces. The observed positive trends are consistent with increasing precipitation during the study period (Fig. 3b). Nevertheless, it is essential to note that the amplitude of the increasing trends in precipitation is an order of magnitude lesser than that of TWS (note the distinct units of the trend in the color-bar presented in Fig. 3). Despite the heightened concentration of precipitation in the southern regions of YRB and coastal provinces, such as Shanghai, Jiangxi, and Hunan, the positive trends in runoff, which generally correspond with the spatial distribution of the precipitation (Fig. 3d), offset the growth of TWS in these areas. In addition, the trends in evapotranspiration are relatively small to be responsible for YRB's TWS changes (Fig. 3c).

Figure 4 shows the annual changes and trends in TWS, precipitation, evapotranspiration, and runoff for YRB and its nine sub-regions defined in this study. Overall, TWS changes in YRB exhibit a statistically significant increasing trend at a rate of 0.41 cm/yr. In comparison, the magnitude of the precipitation trend (0.09 cm/yr) accounts for about 22% of the TWS trend (Table 3). No significant trend observed in the basin-averaged evapotranspiration, whereas runoff reveals a significant positive trend (0.05 cm/yr) during the study period. Specifically, seven of the nine sub-regions demonstrate a significant increase in TWS, with the largest trend of 0.82 cm/yr in CQ and the lowest of 0.2 cm/yr in JZHW. Of the seven regions, only three exhibit significant precipitation trends at rates of 0.05 cm/yr, 0.13 cm/yr, and 0.13 cm/yr in SXY, GZ, and GH, respectively. The observed increasing trends of TWS in GHS (0.05 cm/yr) and JX (0.37 cm/yr) are not statistically significant. Although precipitation in JX increased significantly at a rate of 0.16 cm/yr from 2003 to 2022, the suddenly reduced TWS after 2016, likely caused by the increasing runoff (0.13 cm/yr) (Fig. 4), leads to a non-significant trend in TWS over there. In addition, no significant trends in evapotranspiration are observed for these sub-regions. The increasing trends in runoff over CQ (0.06 cm/yr), GZ (0.11 cm/yr), and GH (0.11 cm/yr) primarily result from the increasing precipitation (Fig. 4).

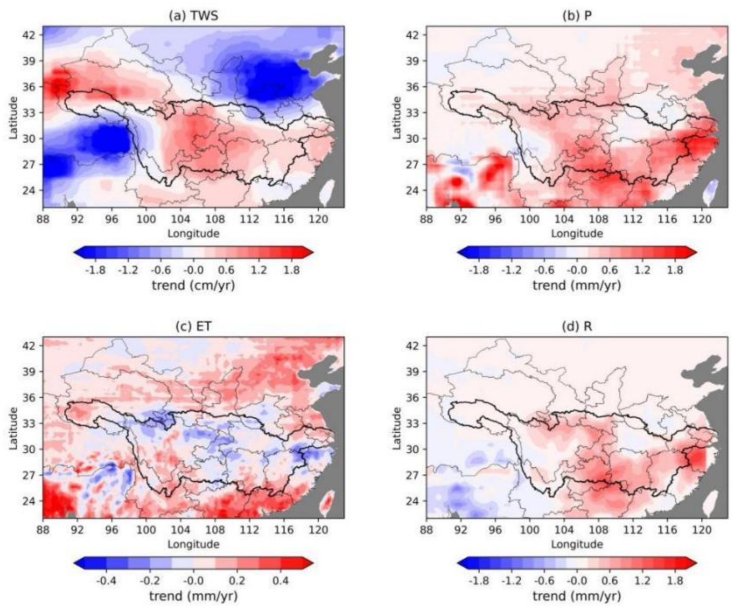

Fig. 3. Spatial trends in (**a**) TWS (cm/yr), (**b**) precipitation (P, mm/yr), (**c**) evapotranspiration (ET, mm/yr), and (**d**) runoff (R, mm/yr) over YRB for the period 2002-2022.

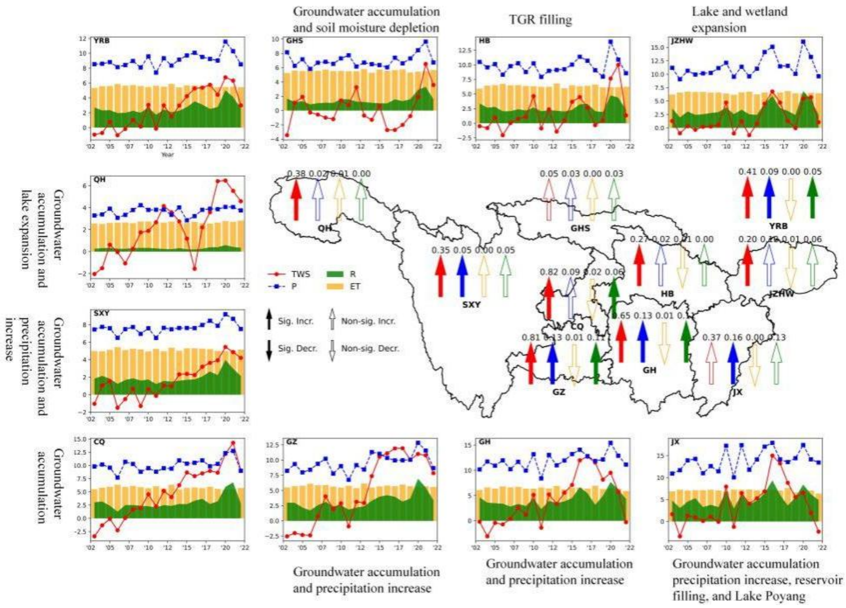

Fig. 4. Annual changes and trends (cm/yr) in TWS, precipitation (P), evapotranspiration (ET), and runoff (R) over YRB and its nine sub-regions for the period 2003-2022. The x-axis represents two-digit years, while the y-axis indicates annual changes in TWS, P, ET and R in centimeters. The upward and downward arrows signify increasing (Incr.) and decreasing (Decr) trends, respectively, with statistically significant (Sig.) trends at a 95% confidence level filled with distinctive colors. A brief explanation of the factors contributing to the trends in TWS within each study region is provided.

Owing to the influences of the East Asian Summer Monsoon and the South China Sea Summer Monsoon, observable annual cycles are evident in both precipitation and TWS for YRB (Fig. S12). The monsoon season, spanning from June to September, is characterized by a substantial increase in precipitation, thereby contributing significantly to TWS changes. Nevertheless, the monthly trends across the years show that the most pronounced increase in TWS occurs during the non-monsoon season, specifically from October to May (Fig. 5a), during which precipitation does not exhibit significant trends, except for March. Noticeable precipitation trends emerge in March, June, and September, with rates of 1.4 cm/yr, 2.2 cm/yr, and 2.2 cm/yr, respectively. In contrast, statistically significant increasing trends in TWS are discernible in all months except August and September. Similar monthly trends in TWS are observed in GZ, QH, SXY, and CQ (Fig. 5d, h-j). In the GH, HB, and JZWH regions, noteworthy TWS trends are observed from December to April despite the absence of discernible increasing trends in precipitation (Fig. 5c, e, and g). Furthermore, GHS and JX regions generally show no statistically significant positive trends in TWS and precipitation across all months (Fig. 5b and f)). These findings indicate the increase in TWS cannot be directly attributed to precipitation.

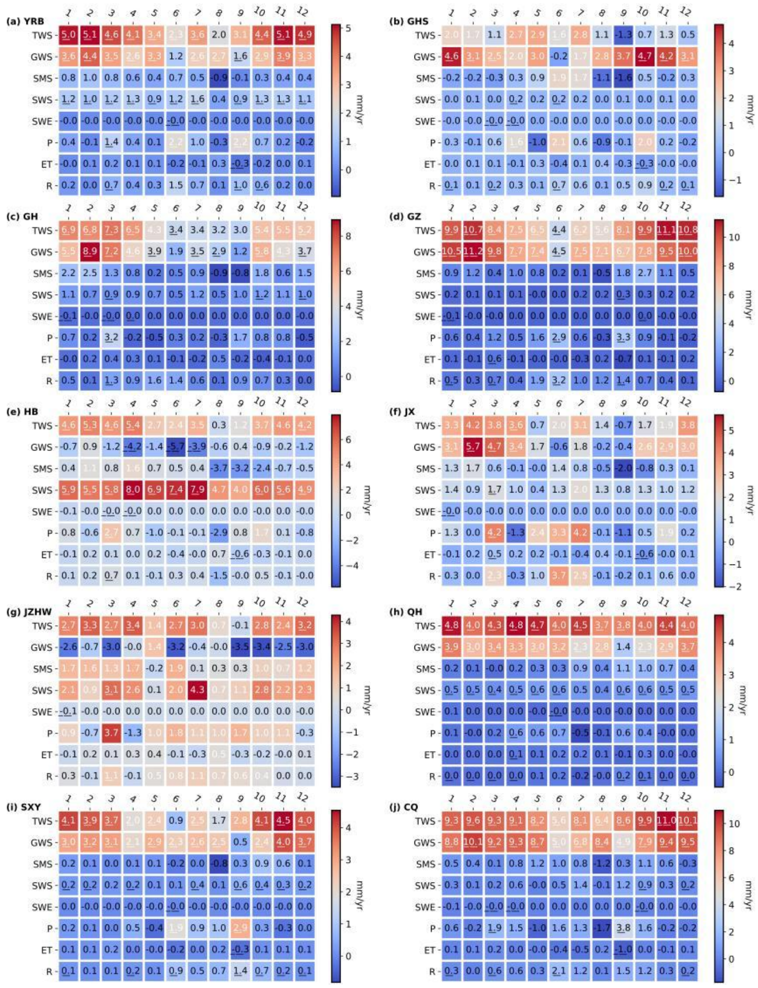

Fig. 5. Monthly trends in precipitation (P), evapotranspiration (ET), runoff (R), TWS, SWE, SWS, SMS, and GWS for YRB and its nine sub-regions. The underline signifies significant trends and correlations at the 95% confidence interval.

To further quantify the contributions of precipitation, evapotranspiration, and runoff to TWS changes, we calculate the trend amplitude ratios by comparing the trends in these variables with respect to TWS. Precipitation predominantly accounts for the escalating rates observed in GHS and JZWH, contributing approximately 60% and 65%, respectively. However, in regions such as SXY, CQ, GZ, and GH, where TWS demonstrates relatively substantial positive trends, precipitation contributes less than 20% (Table 3). This further suggests that precipitation is not the direct factor driving the increase in TWS in these areas. Additionally, the trend amplitude ratios of evapotranspiration to TWS are less than 5%, while runoff contributes prominently in GHS (60%) and JX (35.14%). Therefore, the observed non-significant increasing trends in TWS within these specific regions can be partly attributed to the high runoff ratios, consistent with Figs. 3-4.

Table 3. Percentage (%) of trends in precipitation (P), evapotranspiration (ET), runoff (R), SWE, SWS, SMS, and GWS to trends in TWS over YRB and its nine sub-regions.

	YRB	QH	SXY	GHS	CQ	GZ	HB	GH	JZHW	JX
P	21.95	5.26	14.29	60.00	10.98	16.05	7.41	20.00	65.00	43.24
ET	0.00	2.63	0.00	0.00	2.44	1.23	3.70	1.54	5.00	0.00
R	12.20	0.00	14.29	60.00	7.32	13.58	0.00	16.92	30.00	35.14
SWE	0.00	0.00	0.00	0.00	0.00	0.00	0.00	0.00	0.00	0.00
SWS	29.27	13.16	8.57	20.00	6.10	2.47	218.52	18.46	110.00	40.54
SMS	2.44	13.16	5.71	500.00	2.44	9.88	18.52	27.70	90.00	48.65
GWS	60.98	78.95	80.00	360.00	84.15	98.77	66.67	69.23	170.00	113.51

4.2. Trends in water storage components

In YRB, SWE is predominantly concentrated in the source region, in which spatially consistent negative trends are observed (Fig. 6a). These trends are attributed to rising temperatures associated with global warming (Li et al., 2023). The trend map of SWS generally aligns with the map of lakes and reservoirs within YRB (Fig. 2a-b). For example, apparent trends in SWS are observed in TGR and the three largest lakes (Fig. 6b). The observed increasing trends in SWS in YRB are primarily attributable to the rising number of reservoirs (Rodell et al., 2018). As for SMS, positive trends are observed in the provinces of GZ, Hunan, Jiangxi, and Yangtze River Delta, whereas negative trends are concentrated in Sichuan, parts of CQ, parts of Hubei and Anhui provinces (Fig. 6c). These declining trends are highly likely caused by intensive agricultural activities, given that the agricultural yields of these regions rank among the top four within YRB (http://www.stats.gov.cn/sj/ndsj). Compared to SWE, SWS, and SMS, GWS within YRB displays a substantial positive trend in amplitude, except in instances where significant increasing trends are observed in SWS. This implies that surface water bodies in YRB are actively intercepting water reserves. Negative trends are also identified in the western Sichuan province, attributed to reduced precipitation, as reported by Jing et al. (2020) and Xiong et al. (2022). In addition, the trend map of GWS closely mirrors the trend map of TWS in Fig. 3a, indicating that the increased TWS within YRB primarily results from the rise in GWS, which is consistent with the studies conducted by Chao et al. (2023) and Rodell et al. (2018).

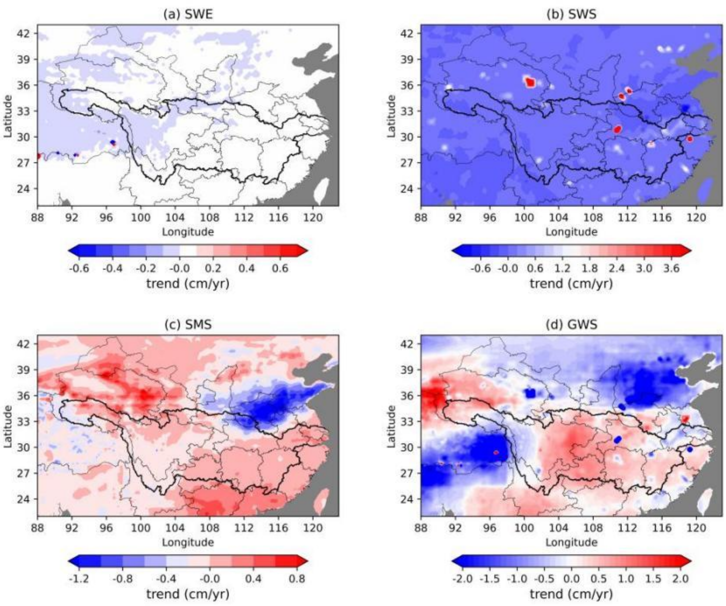

Fig. 6. Spatial trends in (**a**) SWE, (**b**) SWS, (**c**) SMS, and (**d**) GWS over YRB. The trends in SWS and GWS are calculated for the period 2002-2019, whereas those in SWE and SMS are calculated for the period 2002-2022.

Figure 7 illustrates the annual changes and trends in SWE, SWS, SMS, and GWS for YRB and its nine sub-regions. GWS and SWS exhibit statistically significant increasing trends for the whole basin, with respective rates of 0.25 cm/yr and 0.12

cm/yr, while SWE and SMS show minuscule trends. Specifically, SWE within YRB displays negligible trends, even in QH. Statistically significant positive and negative trends in SMS are only discerned in GH and GHS, with rates of 0.18 cm/yr and 0.25 cm/yr, respectively. The escalating trend in GHS is ascribed to an augmentation in precipitation at a rate of 0.13 cm/yr, while the decline in SMS over GHS is likely caused by a relatively high consumption of subsurface water (Figs. 1 and 2c-d). SMS in JZHW and JX regions shows increasing trends but falls short of the 5% significance level, while other areas manifest marginal trends. As for SWS, increasing trends are found in QH, SXY, CQ, HB, GH, JZHW, and JX, with rates of 0.05 cm/yr, 0.03 cm/yr, 0.05 cm/yr, 0.59 cm/yr, 0.12 cm/yr, 0.22 cm/yr, and 0.15 cm/yr, respectively. These observed trends underscore the spatial distribution of lakes and reservoirs within YRB (Figs. 2a-b). Furthermore, noteworthy positive trends in GWS are discernible in QH, SXY, GHS, CQ, GZ, GH, and JX, with rates of 0.3 cm/yr, 0.28 cm/yr, 0.18 cm/yr, 0.69 cm/yr, 0.8 cm/yr, 0.45 cm/yr, and 0.42 cm/yr, respectively. Significant and non-significant declining trends in GWS are observed in HB (0.18 cm/yr) and JZHW (0.34 cm/yr), respectively. The negative trend observed in HB is presumed to be a consequence of surface water bodies in the region intercepting precipitation. The increasing trends in TWS with YRB are generally attributed to GWS, followed by SWS, except HB and JZHW. This is evident in Table 3, wherein the ratios between the trends in GWS and TWS generally exceed 60% across YRB.

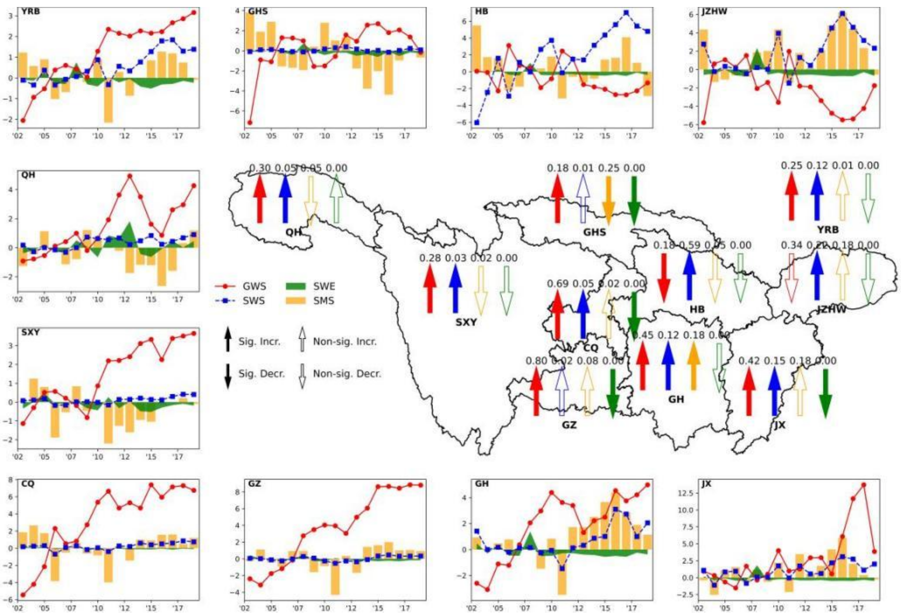

Fig. 7. Annual changes and trends (cm/yr) in SWE, SWS, SMS, and GWS over YRB and its nine sub-regions for the period 2003-2019. The x-axis represents two-digit years, while the y-axis indicates annual changes in GWS, SMS, SWS, and SWE in centimeters. The upward and downward arrows signify increasing (Incr.) and decreasing (Decr) trends, respectively, with statistically significant (Sig.) trends at the 95% confidence interval filled with distinctive colors.

Regarding the monthly trends across the years, GWS in YRB demonstrates statistically positive trends in all months except June. The rates vary from 1.6 cm/yr in September to 4.4 cm/yr in February (Fig. 5a). Notably, these trends predominantly manifest during the non-monsoon season, aligning with the observed trends in TWS. Similarly, SWS experiences significant increasing trends in all months except August within YRB. Comparable positive GWS trends are discernible in various regions, with the exceptions of JZWH and HB, where contrary trends are identified across different months. Furthermore, noteworthy increasing trends in SWS are identified in HB, SXY, and QH. SMS does not reveal any statistically significant trends across the entire basin, whereas the trends in SWE prove to be negligible. These observations substantiate that the increasing TWS within YRB primarily results from increased GWS and SWS.

We further quantify the contributions of individual components to TWS through the use of CCR. Generally, SWE's contributions are less than 1%, with relatively higher contributions noted in high-altitude and high-latitude regions, such as QH, SXY, and GHS (Figs. 8a and e). As for SWS, relatively substantial contributions are observed in JZHW, HB, and CQ, where a considerable number of lakes and reservoirs are situated (Figs. 2a-b). Conversely, SWS accounts for less than 20% of TWS in other regions. The median contributions of SMS and GWS surpass 30% and 40%, respectively (Figs. 8c-d and g-h). In YRB, SMS and GWS contribute comparably concerning the amplitude. The most noteworthy and least significant contributions of SMS are discerned in GHS and CQ, exhibiting median CCR values greater than 50% and 30%, respectively. The observed CCR values for GWS in YRB, SXY, GH, JZHW, JX, HB, and GHS demonstrate similar variations, ranging from 40% to 50%. The highest and lowest contributions are identified in GZ and CQ, displaying median CCR values exceeding 50%.

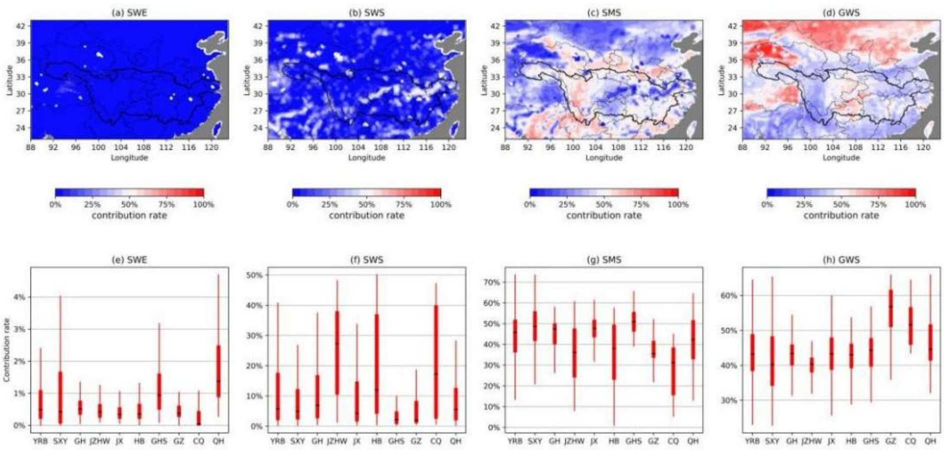

Fig. 8. Map of contribution rates of (**a**) SWE, (**b**) SWS, (**c**) SMS, and (**d**) GWS to TWS over YRB, with (**e-h**) box-plots showing the statistical results for YRB and its nine sub-regions.

4.3. Influence of large lakes and reservoirs on YRB's TWS

The changes in TWS within YRB are influenced by several signals, such as those around the three largest lakes and TGR, as well as the South-to-North Water Diversion (SNWD) project. To assess their potential influence on the dynamics of

TWS in YRB and ensure a fair comparison, we convert TWS, SWS, and reservoir water storage (Res) into volume anomalies by the respective areas of the regions where the water bodies are situated. As the water level of the TGR steadily rose to its target level of approximately 175 meters by the end of the year 2011 and entered into its normal operational phase, the volume anomaly of the TGR showcases a noteworthy positive trend of 1.04 km^3 /yr from 2004 to 2019 (Fig. 9a). During this period, TWS, SWS, and Res in HB experienced increases at rates of 0.52 km^3/yr, 0.91 km^3/yr, and 0.72 km^3/yr, respectively. These trends generally display a consistent increasing pattern with that of the TGR. Therefore, the observed rise in TWS in HB is primarily ascribed to the impact of TGR. The lower trend observed in TWS compared to SWS and Res also indicates the interception functions of surface water bodies. This effect contributes to a decrease in GWS at a rate of 0.18 cm/yr, equivalent to 0.33 km^3/yr, as observed in the HB (Fig. 7). Notably, this value is consistent with the observed trend difference between TWS and Res. In addition, the water transferred by the SNWD project registered an increase at a rate of 1.28 km^3/yr, indicating that the project is poised to substantially influence water storage in HB. However, it is essential to exercise caution in interpreting the impact of SWND, given the relatively short period covered by the analyzed data and the distinct mean field used to compute the volume anomaly (2015-2019) in comparison to TWS, SWS, and Res (2004-2009).

Regarding the influence of Lakes Dongting and Taihu, they exhibit limited influence on the increased TWS in GH and JZWH, respectively, reflected in their low increasing rates of both 0.1 km^3/yr (Fig. 10b and d). SWS in JZWH show comparable trends with TWS, implying that other surface water bodies together lead to increased TWS. Nevertheless, Lake Poyang exhibits a relatively high influence on JX's TWS. Fig. 10c shows that the volume of Lake Poyang has marked inter-annual variations, correlating well with precipitation. From 2003 to 2019, Lake Poyang revealed an increasing rate of 0.48 km^3/yr, accounting for about 30% of the trend observed in TWS in JX. Due to the unique geological location of Lake Poyang, it functions as a massive natural reservoir, playing a crucial role in regulating floods within YRB. JX can be envisioned as a vast basin tilting towards Lake Poyang, where the five major water systems within the province converge and discharge into the Yangtze River. In times of heavy rainfall within JX, the runoff from these five water systems passes through Lake Poyang before ultimately joining the Yangtze River (Liu et al., 2020; Xu et al., 2020). Therefore, at an annual scale, Poyang Lake may exert a higher influence on JX's water storage than SWS and Res (Fig. 10c).

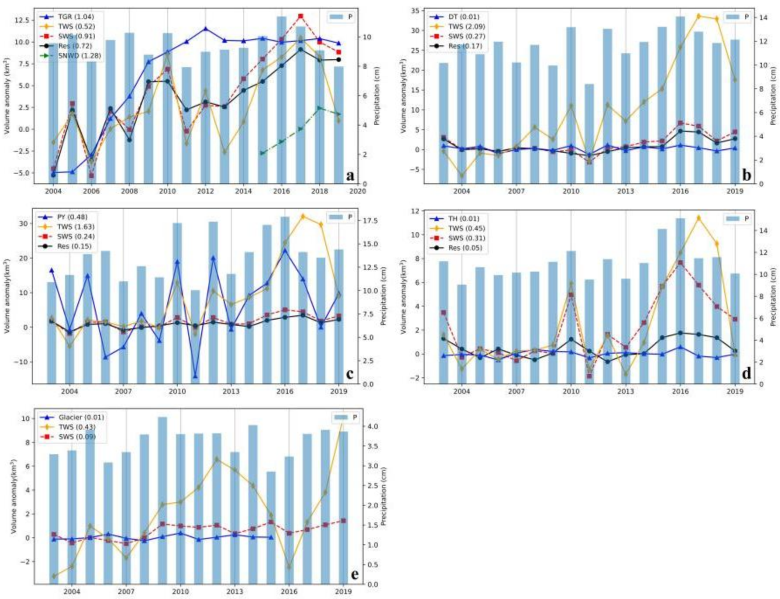

Fig. 9. Annual volume anomalies of TWS, SWS, reservoir (Res), South-to-North-Water-Diversion (SWND) project, TGR, Dongting (DT) lake, Poyang (PY) lake, Taihu (TH) lake, and glaciers. The volume anomaly of TWS, SWS, Res and glacier are computed by multiplying the equivalent water heights by the area of (**a**) HB, (**b**) GH, (**c**) JX, (**d**) JZWH, and (**e**) QH, respectively, with annual mean precipitation series shown in the right axis. The numbers in the bracket are the trends in km^3/yr.

5. Discussion

Precipitation, serving as the direct recharge for TWS changes, has been reported in previous studies as the key factor behind the observed increases in TWS in various regions, even in areas where precipitation does not exhibit significant trends (e.g., Awang et al., 2014; Rodell et al., 2018; Zhang et al., 2019b; Chao et al., 2023). However, within YRB, we have shown that the observed amplitude of trends in precipitation is notably inferior to that in TWS (Figs. 3-4), suggesting precipitation is not a direct factor contributing to the augmentation of TWS in YRB. Figs. 5-8 demonstrate that the increased TWS primarily stems from increased GWS. Notably, the GWS for the current month is typically replenished by the precipitation occurring in the same month, primarily through infiltration. Additionally, there is a partial contribution from the residual GWS from the preceding month (Hipel & McLeod, 1994). This is evident from Fig. 10, which shows a sine exponential decay observed in the autocorrelation plot of each GWS time series within YRB and a significant positive cut-off at lag 1 in the partial autocorrelation plot. This strongly implies that the time series of GWS conforms to a first-order autoregressive model, confirming the contribution of GWS from the previous month to that for the current month. In addition, Fig. 5 reveals that the most significant increase in TWS occurs during a relatively low precipitation period. Therefore, the continuous accumulation of GWS from the preceding month contributes to the observed augmentation in GWS (Fig. 4). Additionally, the predominant source of water within YRB originates mostly (exceeding 90%) from SWS (Fig. 1), thereby resulting in minimal depletion of GWS. The cumulative effect of these factors manifests in an increase of GWS and thus TWS in QH, SXY, CQ, GZ, GH, and JX (Fig. 4). However, the observed significant and non-significant decreasing trends in GWS in HB and JZWH are highly likely attributed to water interception in surface water bodies because SWS in HB and JZWH exhibits significant positive trends at a rate of 0.59 cm/yr and 0.22 cm/yr, respectively (Fig. 7). Furthermore, precipitation does not exhibit decreasing trends (Fig. 4) in these two regions, and the discernible absence of a substantial depletion of GWS, as depicted in Fig. 1.

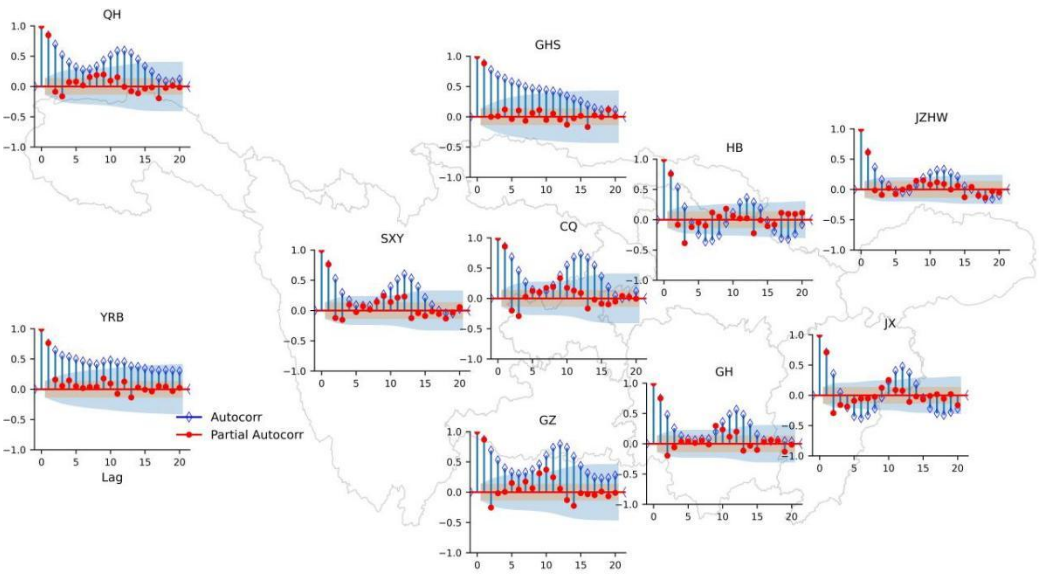

Fig. 10. The autocorrelation and partial autocorrelation of GWS for YRB and its nine sub-regions, with the light blue and red envelopes denoting the 95% confidence intervals.

In addition to GWS, the rising SWS within YRB also plays an important role in the overall increase in TWS. Specifically, in QH, glacier thawing contributes only about 2% to the expanding TWS (Fig. 9e), while lake expansion accounts for a more substantial 21% (Fig. S13). The increasing SWS in SXY and JX result from the increasing water in reservoir and river, whereas significant positive trends in SWS observed in CQ and GH are attributable to the rise in river water storage (Fig. S13). Furthermore, the observed increasing trends in TWS in JZWH are primarily attributable to the wetland and lakes (Fig. S13), whereas TGR contributes to the increasing water storage in HB (Fig. 4). Significant increasing trends in SWS in GZ, GH, and JX are partly explained by the significant increasing trends observed in precipitation (Fig. 4). In addition, Lake Poyang also demonstrates a significant contribution to the increased TWS in JX. The non-significant trend in TWS observed in GHS is balanced by the GWS accumulation (0.18 cm/yr) and SMS depletion (-0.25 cm/yr) (Figs. 4 and 7). Overall, the observed increasing trends in TWS within YRB result from GWS accumulation, followed by the increasing SWS (Fig. 4).

6. Conclusion

In this study, we reveal the drivers of TWS changes in YRB using multisource data from 2002 to 2022. The key findings are:

1. Most YRB demonstrates notable upward trends in TWS, with the central region exhibiting particularly significant increases. The trends observed in precipitation are an order of magnitude lower than those observed in TWS, suggesting precipitation is not a direct factor contributing to TWS increases.

2. The increasing TWS within YRB is attributed to the rising GWS in QH, SXY, CQ, GZ, GH, and JX, along with the increasing SWS in HB and JZHW. The increasing GWS within YRB primarily results from the cumulative increase in GWS combined with minimal depletion of groundwater resources. The increasing SWS in HB results from the TGR filling, whereas the observed increasing trends in SWS in JZWH are ascribed to the lake and wetland expansion. The relatively balanced TWS changes observed in GHS are caused by the GWS accumulation and SMS consumption.

3. The increasing precipitation in SXY, GZ, GH, and JX contributes to the increase of TWS, accounting for about 14%, 16%, 20%, and 43%, respectively. Lake Poyang contributes to approximately 30% of the observed trend in TWS in JX, while the influence of Lakes Dongting and Taihu on the respective region's TWS is comparatively limited. In addition, the observed increasing trends in SWS in QH is a consequence of the lake expansion, with limited influence from glacier thawing.

Declaration of Competing Interest

We declare that there are no known competing financial interests or personal relationships that could have appeared to influence the research presented within this manuscript.

Acknowledgments

This work was primarily supported by the National Natural Science Foundation of China (Grant No. 42274005 and Grant No. 42192532) and the China Scholarship Council (Grant No. 202306260241).

Open Research

The data collected as part of this work are publicly available in Zenodo (Wang, 2024). The data were analyzed using Python version 3.8 (Van Rossum & Drake, 2009). Figures were made with Matplotlib version 3.5.1 (Hunter, 2007), available under the Matplotlib license at https://matplotlib.org/. Maps were created through Cartopy version 0.21.0 (Elson et al., 2021).

References

Agutu, N. O., Awange, J. L., Ndehedehe, C., Kirimi, F., & Kuhn, M. (2019). GRACE-derived groundwater changes over Greater Horn of Africa: Temporal variability and the potential for irrigated agriculture. Science of the Total Environment, 693, 133467. https://doi.org/10.1016/j.scitotenv.2019.07.273

Arsenault, R., Brissette, F., Martel, J. L., Troin, M., Lévesque, G., Davidson-Chaput, J., Gonzalez, M. C., Ameli, A., & Poulin, A. (2020). A comprehensive, multisource database for hydrometeorological modeling of 14,425 North American watersheds. Scientific Data, 7(1), 1–12. https://doi.org/10.1038/s41597-020-00583-2

Awange, J. (2020). Lake victoria monitored from space. In Lake Victoria Monitored From Space. https://doi.org/10.1007/9783030605513

Awange, J. (2021). The Nile Waters: Weighed from Space. In The Nile Waters: Weighed from Space. https://doi.org/10.1007/978-3-030-64756-8

Awange, J. L., Fleming, K. M., Kuhn, M., Featherstone, W. E., Heck, B., & Anjasmara, I. (2011). On the suitability of the 4°×4° GRACE mascon solutions for remote sensing Australian hydrology. Remote Sensing of Environment, 115(3), 864–875. https://doi.org/10.1016/j.rse.2010.11.014

Awange, J. L., Hu, K. X., & Khaki, M. (2019). The newly merged satellite remotely sensed, gauge and reanalysis-based Multi-Source Weighted-Ensemble Precipitation: Evaluation over Australia and Africa (1981–2016). Science of the Total Environment, 670, 448–465. https://doi.org/10.1016/j.scitotenv.2019.03.148

Awange, J. L., Anyah, R., Agola, N., Forootan, E., & Omondi, P. (2013). Potential impacts of climate and environmental change on the stored water of Lake Victoria Basin and economic implications. 49(October), 8160–8173. https://doi.org/10.1002/2013WR014350

Awange, J. L., Forootan, E., Fleming, K., & Odhiambo, G. (2014). Dominant Patterns of Water Storage Changes in the Nile Basin During 2003-2013. Remote Sensing of the Terrestrial Water Cycle, 9781118872031, 367–381. https://doi.org/10.1002/9781118872086.ch22

Beaudoing, H., & Rodell, M. NASA/GSFC/HSL (2020), GLDAS Noah Land Surface Model L4 monthly 0.25 x 0.25 degree V2.1, Greenbelt, Maryland, USA, Goddard Earth Sciences Data and Information Services Center (GES DISC) [Dataset], Accessed: [2023-01-07], https://doi.org/10.5067/SXAVCZFAQLNO

Chao, N., Chen, G., & Wang, Z. (2020). Impact of Eastern Tibetan Plateau Glacier Melt on Land Water Storage Change across the Yangtze River Basin. Journal of Hydrologic Engineering, 25(3), 1–14. https://doi.org/10.1061/(asce)he.1943-5584.0001882

Chao, N., Jin, T., Cai, Z., Chen, G., Liu, X., Wang, Z., & Yeh, P. J. F. (2021). Estimation of component contributions to total terrestrial water storage change in the Yangtze river basin. Journal of Hydrology, 595(June 2020), 125661. https://doi.org/10.1016/j.jhydrol.2020.125661

Chao, N., Li, F., Yu, N., Chen, G., Wang, Z., Ouyang, G., & Yeh, P. J. F. (2023). Divergent spatiotemporal variability of terrestrial water storage and eight hydroclimatic components over three different scales of the Yangtze River basin. Science of the Total Environment, 879(December 2022), 162886. https://doi.org/10.1016/j.scitotenv.2023.162886

Che, T., Dai, L., & Li, X. (2015). Long-term series of daily snow depth dataset in China (1979-2020,2012-2023). National Tibetan Plateau / Third Pole Environment Data Center. https://doi.org/10.11888/Geogra.tpdc.270194.

Chen, J., Tapley, B., Rodell, M., Seo, K. W., Wilson, C., Scanlon, B. R., & Pokhrel, Y. (2020). Basin-Scale River Runoff Estimation From GRACE Gravity Satellites, Climate Models, and In Situ Observations: A Case Study in the Amazon Basin. Water Resources Research, 56(10), 1–21. https://doi.org/10.1029/2020WR028032

Dai, Z., Du, J., Li, J., Li, W., & Chen, J. (2008). Runoff characteristics of the Changjiang River during 2006: Effect of extreme drought and the impounding of the Three Gorges Dam. Geophysical Research Letters, 35(7), 1–6. https://doi.org/10.1029/2008GL033456

Deng, H., Chen, Y., & Chen, X. (2022). Driving factors and changes in components of terrestrial water storage in the endorheic Tibetan Plateau. Journal of Hydrology, 612(PC), 128225. https://doi.org/10.1016/j.jhydrol.2022.128225

Elson, P., Sales de Andrade, E., Lucas, G., May, R., Hattersley, R., Campbell, E., Dawson, A., Raynaud, S., scmc72, Little, B., Snow, A. D., Donkers, K., Blay, B., Killick, P., Wilson, N., Peglar, P., lbdreyer, Andrew, Szymaniak, J., Berchet, A., Bosley, C., Davis, L., Filipe, Krasting, J., Bradbury, M., Kirkham, D., stephenworsley, Clément, Caria, G., & Hedley, M.: SciTools/cartopy: v0.21.0, Zenodo [Code], https://doi.org/10.5281/zenodo.1182735, 2021.

Felfelani, F., Wada, Y., Longuevergne, L., & Pokhrel, Y. N. (2017). Natural and human-induced terrestrial water storage change: A global analysis using hydrological models and GRACE. Journal of Hydrology, 553, 105–118. https://doi.org/10.1016/j.jhydrol.2017.07.048

Feng, T., Shen, Y., Wang, F., Chen, Q., & Ji, K. (2023). Spatiotemporal variability and driving factors of the shallow soil moisture in North China during the past 31 years. Journal of Hydrology, 619(February), 129331. https://doi.org/10.1016/j.jhydrol.2023.129331

Feng, T., Shen, Y., Chen, Q., Wang, F., & Zhang, X. (2022). Groundwater storage change and driving factor analysis in north china using independent component decomposition. Journal of Hydrology, 609(July 2021), 127708. https://doi.org/10.1016/j.jhydrol.2022.127708

Frappart, F., Papa, F., Güntner, A., Tomasella, J., Pfeffer, J., Ramillien, G., Emilio, T., Schietti, J., Seoane, L., da Silva Carvalho, J., Medeiros Moreira, D., Bonnet, M. P., & Seyler, F. (2019). The spatio-temporal variability of groundwater storage in the Amazon River Basin. Advances in Water Resources, 124(December 2018), 41–52. https://doi.org/10.1016/j.advwatres.2018.12.005

Fu, J., Gong, Y., Zheng, W., Zou, J., Zhang, M., Zhang, Z., Qin, J., Liu, J., & Quan, B. (2022). Spatial-temporal variations of terrestrial evapotranspiration across China from 2000 to 2019. Science of the Total Environment, 825, 153951. https://doi.org/10.1016/j.scitotenv.2022.153951

Gao, S., Li, Z., Chen, M., Lin, P., Hong, Z., Allen, D., Neeson, T., & Hong, Y. (2021). Spatiotemporal variability of global river extent and the natural driving factors revealed by decades of Landsat observations, GRACE gravimetry observations, and land surface model simulations. Remote Sensing of Environment, 267(October), 112725. https://doi.org/10.1016/j.rse.2021.112725

Harris, I., Osborn, T. J., Jones, P., & Lister, D. (2020). Version 4 of the CRU TS monthly high-resolution gridded multivariate climate dataset. Scientific Data, 7(1), 1–18. https://doi.org/10.1038/s41597-020-0453-3

Hipel, K. W., & McLeod, A. I. (1994). Time series modelling of water resources and environmental systems. Elsevier.

Hosseini-Moghari, S. M., Araghinejad, S., Ebrahimi, K., Tang, Q., & AghaKouchak, A. (2020). Using GRACE satellite observations for separating meteorological variability from anthropogenic impacts on water availability. Scientific Reports, 10(1), 1–12.

https://doi.org/10.1038/s41598-020-71837-7

Huang, Y., Salama, M. S., Krol, M. S., Su, Z., Hoekstra, A. Y., Zeng, Y., & Zhou, Y. (2015). Estimation of human-induced changes in terrestrial water storage through integration of GRACE satellite detection and hydrological modeling: A case study of the Yangtze River basin. Water Resources Research, 51(10), 8494-8516. https://doi.org/10.1002/2015WR016923

Humphrey, V., Gudmundsson, L., & Seneviratne, S. I. (2016). Assessing Global Water Storage Variability from GRACE: Trends, Seasonal Cycle, Subseasonal Anomalies and Extremes. Surveys in Geophysics, 37(2), 357–395. https://doi.org/10.1007/s10712-016-9367-1

Hunter, J. D. (2007). Matplotlib: A 2d graphics environment. Computing in Science & Engineering, 9(3), 90 – 95. https://doi.org/10.1109/MCSE.2007.55

Li, J., Wang, G., Li, K., Li, Y., Guo, L., & Song, C. (2023). Impacts of climate change and freeze–thaw cycles on water and sediment fluxes in the headwater region of the Yangtze River, Qinghai–Tibet Plateau. Catena, 227(February), 107112. https://doi.org/10.1016/j.catena.2023.107112

Li, Q., Liu, X., Zhong, Y., Wang, M., Bai, H., & Xiao, C. (2023). Assessing the interannual and subseasonal variabilities in water storage using multi-source soil moisture products and GRACE/GRACE-FO satellites and its applications. Journal of Hydrology, 627(PB), 130439. https://doi.org/10.1016/j.jhydrol.2023.130439

Jing, W., Zhao, X., Yao, L., Jiang, H., Xu, J., Yang, J., & Li, Y. (2020). Variations in terrestrial water storage in the Lancang-Mekong river basin from GRACE solutions and land surface model. Journal of Hydrology, 580(March 2019), 124258. https://doi.org/10.1016/j.jhydrol.2019.124258

Li, Y., Yan, D., Peng, H., & Xiao, S. (2021). Evaluation of precipitation in CMIP6 over the Yangtze River Basin. Atmospheric Research, 253(December). https://doi.org/10.1016/j.atmosres.2020.105406

Liu, F., Kang, P., Zhu, H., Han, J., & Huang, Y. (2021). Analysis of spatiotemporal groundwater-storage variations in China from Grace. Water (Switzerland), 13(17). https://doi.org/10.3390/w13172378

Liu, H., Zheng, L., Jiang, L., & Liao, M. (2020). Forty-year water body changes in Poyang Lake and the ecological impacts based on Landsat and HJ-1 A/B observations. Journal of Hydrology, 589(June), 125161. https://doi.org/10.1016/j.jhydrol.2020.125161

Liu, Y., Wu, G., & Zhao, X. (2013). Recent declines in China's largest freshwater lake: Trend or regime shift? Environmental Research Letters, 8(1). https://doi.org/10.1088/1748-9326/8/1/014010

Long, D., Shen, Y., Sun, A., Hong, Y., Longuevergne, L., Yang, Y., Li, B., & Chen, L. (2014). Drought and flood monitoring for a large karst plateau in Southwest China using extended GRACE data. Remote Sensing of Environment, 155, 145–160.

https://doi.org/10.1016/j.rse.2014.08.006

Long, D., Yang, W., Scanlon, B. R., Zhao, J., Liu, D., Burek, P., Pan, Y., You, L., & Wada, Y. (2020). South-to-North Water Diversion stabilizing Beijing's groundwater levels. Nature Communications, 11(1). https://doi.org/10.1038/s41467-020-17428-6

Long, D., Yang, Y., Wada, Y., Hong, Y., Liang, W., Chen, Y., Yong, B., Hou, A., Wei, J., & Chen, L. (2015). Deriving scaling factors using a global hydrological model to restore GRACE total water storage changes for China's Yangtze River Basin. Remote Sensing of Environment, 168, 177–193. https://doi.org/10.1016/j.rse.2015.07.003

Loomis, B. D., Luthcke, S. B., & Sabaka, T. J. (2019). Regularization and error characterization of GRACE mascons. Journal of Geodesy, 93(9), 1381–1398. https://doi.org/10.1007/s00190-019-01252-y

Lu, R., Xu, K., Chen, R., Chen, W., Li, F., & Lv, C. (2022). Heat waves in summer 2022 and increasing concern regarding heat waves in general. Atmospheric and Oceanic Science Letters, 16(September 2022), 100290. https://doi.org/10.1016/j.aosl.2022.100290

Martens, B., Miralles, D. G., Lievens, H., Van Der Schalie, R., De Jeu, R. A. M., Fernández-Prieto, D., Beck, H. E., Dorigo, W. A., & Verhoest, N. E. C. (2017). GLEAM v3: Satellite-based land evaporation and root-zone soil moisture. Geoscientific Model Development, 10(5), 1903–1925. https://doi.org/10.5194/gmd-10-1903-2017

Meshram, S. G., Kahya, E., Meshram, C., Ghorbani, M. A., Ambade, B., & Mirabbasi, R. (2020). Long-term temperature trend analysis associated with agriculture crops. Theoretical and Applied Climatology, 140(3–4), 1139–1159. https://doi.org/10.1007/s00704-020-03137-z

Ministry of Water Resources of the People's Republic of China. Bulletin of Water Resources in the Yangtze River Basin and Southwest Rivers 2003-2022 (Ministry of Water Resources of the People's Republic of China, 2022). http://www.cjw.gov.cn

Müller Schmied, H., Caceres, D., Eisner, S., Flörke, M., Herbert, C., Niemann, C., Asali Peiris, T., Popat, E., Theodor Portmann, F., Reinecke, R., Schumacher, M., Shadkam, S., Telteu, C. E., Trautmann, T., & Döll, P. (2021). The global water resources and use model WaterGAP v2.2d: Model description and evaluation. Geoscientific Model Development, 14(2), 1037 – 1079. https://doi.org/10.5194/gmd-14-1037-2021

Muñoz-Sabater, J. (2019): ERA5-Land monthly averaged data from 1950 to present. Copernicus Climate Change Service (C3S) Climate Data Store (CDS). https://doi.org/10.24381/cds.68d2bb30 (Accessed on 10-11-2023)

Panda, D. K., & Wahr, J. (2016). Spatiotemporal evolution of water storage changes in I ndia from the updated GRACE – derived gravity records. Water Resources Research, 52(1), 135-149. https://doi.org/10.1002/2015WR017797

Rodell, M., Famiglietti, J. S., Wiese, D. N., Reager, J. T., Beaudoing, H. K., Landerer, F. W., & Lo, M. H. (2018). Emerging trends in global freshwater availability. Nature, 557(7707), 651 – 659. https://doi.org/10.1038/s41586-018-0123-1

Rodell, M., Houser, P. R., Jambor, U., Gottschalck, J., Mitchell, K., Meng, C. J., Arsenault, K., Cosgrove, B., Radakovich, J., Bosilovich, M., Entin, J. K., Walker, J. P., Lohmann, D., & Toll, D. (2004). The Global Land Data Assimilation System. Bulletin of the American Meteorological Society, 85(3), 381–394. https://doi.org/10.1175/BAMS-85-3-381

Rodell, M., & Reager, J. T. (2023). Water cycle science enabled by the GRACE and GRACE-FO satellite missions. Nature Water, 1(1), 47–59. https://doi.org/10.1038/s44221-022-00005-0

Save, H., Bettadpur, S., & Tapley, B. D. (2016). High-resolution CSR GRACE RL05 mascons. Journal of Geophysical Research: Solid Earth, 121(10), 7547-7569. http://dx.doi.org/10.1002/2016JB013007

Scanlon, B. R., Z. Zhang, H. Save, D. N. Wiese, F. W. Landerer, D. Long, L. Longuevergne, & J. Chen (2016), Global evaluation of new GRACE mascon products for hydrologic applications, Water Resour. Res., 52,9412–9429, https://doi:10.1002/2016WR019494.

Schumacher, M., Forootan, E., van Dijk, A. I. J. M., Müller Schmied, H., Crosbie, R. S., Kusche, J., & Döll, P. (2018). Improving drought simulations within the Murray-Darling Basin by combined calibration/assimilation of GRACE data into the WaterGAP Global Hydrology Model. Remote Sensing of Environment, 204(March 2017), 212–228. https://doi.org/10.1016/j.rse.2017.10.029

Seka, A. M., Zhang, J., Ayele, G. T., Demeke, Y. G., Han, J., & Prodhan, F. A. (2022). Spatio-temporal analysis of water storage variation and temporal correlations in the East Africa lake basins. Journal of Hydrology: Regional Studies, 41(December 2021), 101094. https://doi.org/10.1016/j.ejrh.2022.101094

Shan, L., Zhang, L., Song, J., Zhang, Y., She, D., & Xia, J. (2018). Characteristics of dry-wet abrupt alternation events in the middle and lower reaches of the Yangtze River Basin and the relationship with ENSO. Journal of Geographical Sciences, 28(8), 1039–1058. https://doi.org/10.1007/s11442-018-1540-7

Sun, Z., Zhu, X., Pan, Y., Zhang, J., & Liu, X. (2018). Drought evaluation using the GRACE terrestrial water storage deficit over the Yangtze River Basin, China. Science of the Total Environment, 634, 727–738. https://doi.org/10.1016/j.scitotenv.2018.03.292

Tangdamrongsub, N., Ditmar, P. G., Steele-Dunne, S. C., Gunter, B. C., & Sutanudjaja, E. H. (2016). Assessing total water storage and identifying flood events over Tonlé Sap basin in Cambodia using GRACE and MODIS satellite observations combined with hydrological models. Remote Sensing of Environment, 181, 162–173. https://doi.org/10.1016/j.rse.2016.03.030

Tangdamrongsub, N., Steele-Dunne, S. C., Gunter, B. C., Ditmar, P. G., & Weerts, A. H. (2015). Data assimilation of GRACE terrestrial water storage estimates into a regional hydrological model of the Rhine River basin. Hydrology and Earth System Sciences, 19(4), 2079–2100. https://doi.org/10.5194/hess-19-2079-2015

Tapley, B. D., Watkins, M. M., Flechtner, F., Reigber, C., Bettadpur, S., Rodell, M., Sasgen, I., Famiglietti, J. S., Landerer, F. W., Chambers, D. P., Reager, J. T., Gardner, A. S., Save, H., Ivins, E. R., Swenson, S. C., Boening, C., Dahle, C., Wiese, D. N., Dobslaw, H., … Velicogna, I. (2019). Contributions of GRACE to understanding climate change. Nature Climate Change, 9(5), 358–369. https://doi.org/10.1038/s41558-019-0456-2

Thomas, A.C., Reager, J.T., Famiglietti, J.S., & Rodell, M. (2014). A GRACE- based water storage deficit approach for hydrological drought characterization. Geophys. Res. Lett. 41, 1537–1545. https://doi.org/10.1002/2014GL059323.

Van Rossum, G. & Drake, F.L., 2009. Python 3 Reference Manual, Scotts Valley, CA: CreateSpace [Code].

Wang, J. (2024). Drivers of water storage changes in the Yangtze River Basin during 2002-2022 (1.0). Zenodo. https://doi.org/10.5281/zenodo.10512888 [Dataset]

Wang, J., & Chen, Y. (2022). Using NARX neural network to forecast droughts and floods over Yangtze River Basin. Natural Hazards, 110(1), 225–246. https://doi.org/10.1007/s11069-021-04944-x

Wang, J., Chen, Y., Wang, Z., & Shang, P. (2020). Drought evaluation over Yangtze River basin based on weighted water storage deficit. Journal of Hydrology, 591(May), 125283. https://doi.org/10.1016/j.jhydrol.2020.125283

Wang, J., Walter, B. A., Yao, F., Song, C., Ding, M., Maroof, A. S., Zhu, J., Fan, C., McAlister, J. M., Sikder, S., Sheng, Y., Allen, G. H., Crétaux, J. F., & Wada, Y. (2022). GeoDAR: georeferenced global dams and reservoirs dataset for bridging attributes and geolocations. Earth System Science Data, 14(4), 1869–1899. https://doi.org/10.5194/essd-14-1869-2022

Wang, S., Zhao, Q., & Pu, T. (2021). Assessment of water stress level about global glacier-covered arid areas: A case study in the Shule River Basin, northwestern China. Journal of Hydrology: Regional Studies, 37(August), 100895. https://doi.org/10.1016/j.ejrh.2021.100895

Wang, X., De Linage, C., Famiglietti, J., & Zender, C. S. (2011). Gravity Recovery and Climate Experiment (GRACE) detection of water storage changes in the Three Gorges Reservoir of China and comparison with in situ measurements. Water Resources Research, 47(12), 1–13. https://doi.org/10.1029/2011WR010534

Wang, Y., Sun, Z., Wu, Q., Fang, J., & Jia, W. (2023). Spatio-temporal variability of terrestrial water storage in the Yangtze River Basin: Response to climate changes. Geodesy and Geodynamics. https://doi.org/10.1016/j.geog.2022.11.006

Wiese, D. N., Yuan, D. N., Boening, C., Landerer, F. W., & Watkins, M. M. (2019). JPL GRACE Mascon Ocean, Ice, and Hydrology Equivalent Water Height RL06 CRI Filtered Version 02. Ver. 02. PO.DAAC, CA, USA. [Dataset] accessed [2023-01-06] at https://doi.org/10.5067/TEMSC-3JC62

Xie, J., Xu, Y. P., Yu, H., Huang, Y., & Guo, Y. (2022). Monitoring the extreme flood events in the Yangtze River basin based on GRACE and GRACE-FO satellite data. Hydrology and Earth System Sciences, 26(22), 5933–5954. https://doi.org/10.5194/hess-26-5933-2022

Xie, P., Yatagai, A., Chen, M., Hayasaka, T., Fukushima, Y., Liu, C., & Yang, S. (2007). A gauge-based analysis of daily precipitation over East Asia. Journal of Hydrometeorology, 8(3), 607–626. https://doi.org/10.1175/JHM583.1

Xie, X., He, B., Guo, L., Miao, C., & Zhang, Y. (2019). Detecting hotspots of interactions between vegetation greenness and terrestrial water storage using satellite observations. Remote Sensing of Environment, 231(June), 111259. https://doi.org/10.1016/j.rse.2019.111259

Xiong, J., Guo, S., Chen, D., Zhong, Y., Liu, B., Abhishek, & Yin, J. (2022). Past and future terrestrial water storage changes in the lower Mekong River basin: The influences of climatic and non-climatic factors. Journal of Hydrology, 612(PC), 128275. https://doi.org/10.1016/j.jhydrol.2022.128275

Xu, G., Wu, Y., Liu, S., Cheng, S., Zhang, Y., Pan, Y., Wang, L., Yu. Dokuchits, E., & Nkwazema, O. C. (2023). How 2022 extreme drought influences the spatiotemporal variations of terrestrial water storage in the Yangtze River Catchment: Insights from GRACE-based drought severity index and in-situ measurements. Journal of Hydrology, 626(PA), 130245. https://doi.org/10.1016/j.jhydrol.2023.130245

Xu, Y., Li, J., Wang, J., Chen, J., Liu, Y., Ni, S., Zhang, Z., & Ke, C. (2020). Assessing water storage changes of Lake Poyang from multi-mission satellite data and hydrological models. Journal of Hydrology, 590(May), 125229. https://doi.org/10.1016/j.jhydrol.2020.125229

Yan, X., Zhang, B., Yao, Y., Yin, J., Wang, H., & Ran, Q. (2022). Jointly using the GLDAS 2 . 2 model and GRACE to study the severe Yangtze flooding of 2020. Journal of Hydrology, 610(March), 127927. https://doi.org/10.1016/j.jhydrol.2022.127927

Yang, L., Wang, L., Zhang, M., Niu, Z., Yao, R., Yu, D., Li, C., & He, Q. (2021a). Variation of water body in Dongting Lake from in situ measurements and MODIS observations in recent decades. International Journal of Digital Earth, 14(8), 959–984. https://doi.org/10.1080/17538947.2021.1907464

Yang, P., Xia, J., Luo, X., Meng, L., & Zhang, S. (2021b). Impacts of climate change-related flood events in the Yangtze River Basin based on multi-source data. Atmospheric Research, 263(July), 105819. https://doi.org/10.1016/j.atmosres.2021.105819

Yang, S. L., Xu, K. H., Milliman, J. D., Yang, H. F., & Wu, C. S. (2015). Decline of Yangtze River water and sediment discharge: Impact from natural and anthropogenic changes. Scientific Reports, 5(November 2014), 1–14. https://doi.org/10.1038/srep12581

Zhang, D., Liu, X., & Bai, P. (2019). Assessment of hydrological drought and its recovery time for eight tributaries of the Yangtze River (China) based on downscaled GRACE data. Journal of Hydrology, 568(November 2018), 592–603. https://doi.org/10.1016/j.jhydrol.2018.11.030

Zhang, G. Q., Xie, H. J., Yao, T. D., & Kang, S. C. (2013). Water balance estimates of ten greatest lakes in China using ICESat and Landsat data. Chinese Science Bulletin, 58(31), 3815–3829. https://doi.org/10.1007/s11434-013-5818-y (in Chinese)

Zhang, G., Yao, T., Chen, W., Zheng, G., Shum, C. K., Yang, K., Piao, S., Sheng, Y., Yi, S., Li, J., O'Reilly, C. M., Qi, S., Shen, S. S. P., Zhang, H., & Jia, Y. (2019a). Regional differences of lake evolution across China during 1960s–2015 and its natural and anthropogenic causes. Remote Sensing of Environment, 221(December 2017), 386–404. https://doi.org/10.1016/j.rse.2018.11.038

Zhang, L., Shen, Y., Chen, Q., & Wang, F. (2023). Influence factors and mechanisms of 2015–2016 extreme flood in Pearl River Basin based on the WSDI from GRACE. Journal of Hydrology: Regional Studies, 47(February), 101376. https://doi.org/10.1016/j.ejrh.2023.101376

Zhang, Y., He, B., Guo, L., Liu, J., & Xie, X. (2019b). The relative contributions of precipitation, evapotranspiration, and runoff to terrestrial water storage changes across 168 river basins. Journal of Hydrology, 579(September), 124194. https://doi.org/10.1016/j.jhydrol.2019.124194

Zheng, S., Zhang, Z., Yan, H., Zhao, Y., & Li, Z. (2023). Characterizing drought events occurred in the Yangtze River Basin from 1979 to 2017 by reconstructing water storage anomalies based on GRACE and meteorological data. Science of the Total Environment, 868(December 2022), 161755. https://doi.org/10.1016/j.scitotenv.2023.161755

Zhou, Z. Q., Xie, S. P., & Zhang, R. (2021). Historic Yangtze flooding of 2020 tied to extreme Indian Ocean conditions. Proceedings of the National Academy of Sciences of the United States of America, 118(12), 1–7. https://doi.org/10.1073/pnas.202225511

Zhu, Y., Liu, S., Yi, Y., Xie, F., Grünwald, R., Miao, W., Wu, K., Qi, M., Gao, Y., & Singh, D. (2021). Overview of terrestrial water storage changes over the Indus River Basin based on GRACE/GRACE-FO solutions. Science of the Total Environment, 799. https://doi.org/10.1016/j.scitotenv.2021.149366